Project no. 606953

MarcoPolo

Monitoring and Assessment of Regional air quality in China using space Observations.

Project Of Long-term sino-european co-Operation

Type of funding scheme: Collaborative Project - Small or medium-scale focused research project
Work programme topics addressed: SPA.2013.3.2-01: Cooperation with third countries

Deliverable D 4.3 (PU)

Part I: Assessment impact updated emission inventories
Part II: PM source apportionment over China

Version: 1.0

Due date of final deliverable: project month 36
Actual submission date: project month 36

Organisation name of lead contractor for this deliverable: TNO

Document Status sheet	
Lead Author	Renske Timmermans (TNO)
Contributing Authors	Richard Kranenburg (TNO), Hans Hooyberghs (VITO)
Reviewed by	
Distribution list	Project partners and EC

Document Change Record			
Date	***Issue***	***Pages affected***	***Description***
13/12/2016	1.0	All	Initial draft
30/01/2017	2.0	All	Updates pictures and separated part I and II

Table of Contents

1. Introduction

In the MarcoPolo project a new emission database for China is constructed based on emission estimates from space observations and the refinement of these emission estimates by spatial downscaling. The new emission inventory is described in the MarcoPolo deliverable 4.2.

Part I of this deliverable describes the impact of the new emission inventory for the existing air quality modelling by comparing two model runs: one with the new MarcoPolo inventory and one with bottom-up MEIC emission inventory provided.

Part II of this report is focusing on the source apportionment of PM2.5 over China. To be able to define effective mitigation strategies it is important to know which source are responsible for high PM levels. We have performed a source apportionment analysis for the entire year 2013 over Eastern China, with special focus on the cities of Beijing and Shanghai. For those cities the contributions from different source sectors and regions have been identified for different periods of the year.

In both parts we make use of the chemistry transport model LOTOS-EUROS and compare the model results with observations from satellites and ground based observations. The model and observations are described in sections 2 and 3

2. Chemistry transport model

LOTOS-EUROS is a three dimensional regional chemistry transport model (CTM) conventionally used for air pollution assessments over Europe. Within recent years the model system has been adapted to allow application to any location in the world, including China (Timmermans et al., 2016). For a detailed model description we refer to Manders et al. (2016) and references therein.
In this study we apply LOTOS-EUROS version 1.10 to investigate the origin of fine particulate matter across China with special emphasis on Beijing and Shanghai and to determine the impact of the updated emission inventory from MarcoPolo.
Land use information is obtained from the Global Land Cover 2000 database (European Commission, Joint Research Centre, 2003, http://www-gem.jrc.it/glc2000GLC2000) and EDGAR v2.4 emission data are used (European Commission et al., 2011) for the regions outside China. In the source apportionment application the Chinese emission data were prescribed using the Multi-resolution Emission Inventory for China (MEIC) (http://www.meicmodel.org). The use of this emission inventory is compared to the use of the MarcoPolo emission inventory for the impact study of the updated emission inventory. The seasonal emission variability is given through the use of the monthly emission files. European sector specific daily and hourly factors (Builtjes, P.J.H., et al., 2003) have been applied to divide the monthly emissions over the days of the week and

hours of the day. These European factors were thought to be similarly appropriate for China (Q. Zhang, personal communication), however current results hint that the assumed diurnal cycle in the emissions may not be appropriate for large cities in China. Natural emissions from sea salt and desert dust are calculated online (see Manders et al., 2016, 2010). The biogenic emission originate from the MEGAN Version 2.04 (Guenther et al., 2006). Wild fire emissions are taken from the operational GFAS product (Kaiser et al., 2012). Due to lack of traffic intensity information and information on agricultural activities we have turned off the dust emission parametrization for traffic resuspension and agricultural activities in China. Secondary organic aerosols (SOA) are not included in the model runs discussed in this report, due to large uncertainties in the VBS scheme and the fact that the source apportionment technique is not yet incorporated for the formation of SOA.

3. Observational data

For evaluation of model results several observational datasets have been used both from satellite as well as in-situ surface instruments.

US Embassy observations

For PM2.5 we have used U.S. Department of State data from the data portal www.stateair.net for the full year of 2013 and 2014 for 5 stations. These air quality data are measured at the U.S. Embassy and consulates in Beijing, Chengdu, Guangzhou, Shanghai and Shenyang using MetOne BAM 1020 and a Ecotech EC9810 monitors. Here we only present results at Beijing and Shanghai. The monitor in Beijing is located at Northeast 3rd Ring Road in the Chaoyang district (39.95N; 116.47E) The monitor in Shanghai is located on the consulate compound on Huai Hai Middle Road (31.21N; 121.44E) inside the inner ring road of Shanghai. Note that State Air observational data are not fully verified or validated but they provide a first means of checking modelled PM2.5 levels and temporal variability. A recent assessment showed that the observed PM levels measured highly correlated with data from other stations in downtown Beijing (Batterman et al., 2016).

Institute of Atmospheric Physics observations in Beijing

This site established by the Institute of Atmospheric Physics (IAP), Chinese Academy of Sciences (CAS), is located in the northern part of Beijing urban city (39.97N; 116.37E; 44 m.a.s.l.), between the north 3rd Ring Road and the north 4th Ring Road, which is an urban area approximately 8 km away from the centre of Beijing. The site was set up according to the US EPA methodological designation (US EPA, 2004) on the rooftop of a two-story building. NOx is measured using a chemiluminescence NOx analyzer (Model 42C/I, Thermo-Fisher Scientific, USA), and for SO2 a pulsed fluorescence SO2 analyzer (Model 43 C/I, Thermo-Fisher Scientific, USA) is used. The concentrations of particles (PM10 and PM2.5) are measured using a TEOM RP1400 (Thermo Scientific, http://www.thermoscientific.com), and the entire system was heated to 50°C, thus, loss of

semivolatile compounds thereby cannot be avoided. Depending on the ammonium nitrate levels and ambient temperatures, up to 25% lower mass concentrations were found for select daily means compared with gravimetric filter measurements. High resolution (5 min averages) data sets of NO2, SO2, PM10 and PM2.5 during 2013 were obtained, and hourly averaged data were used after applying strict data quality control; no data were available on some days due to instrument failure, power failure, programming error, and computer failure. The daily average values were calculated using a minimum of 18 1-h averages.

Shanghai Environmental Monitoring Center observations in Shanghai

The Shanghai Environmental Monitoring Center is the responsible institute for monitoring PM, NO_2 and SO_2 and reporting the air pollution index to the public in Shanghai. SEMC operates and maintains an air quality monitoring network since the 1980s. In this study we used daily averaged values from 8 automatic national control sites approved by the China ***Environmental Protection Bureau, available through the website http://www.semc.com.cn/.*** The stations are located at Pu Tuo, Shi Wu Chang, Hong Kou, Jing An, Shang Shi Da, Yang Pu, Chuan Sha, Pudong and Zhang Jiang. The stations are all located fairly close to each other within 30 km x 15 km area. The average value over all 8 stations is used in the comparisons. SO_2 and NO_2 are monitored by a Teledyne Advanced Pollution Instrumentation UV Fluorescence Analyzer (TAPI) and a Chemiluminescence Analyzer 200E while PM is monitored using TEOM monitors. The data is quality controlled and reported following US EPA guidelines (US EPA, 2004).

Peking University observations in Dezhou and Baoding

Peking University (PKU) conducted four daily $PM_{2.5}$ measurement campaigns in 2013 (July-August, November-December) and 2014 (April, October-November). Two campaign sites were selected in the Huabei area, Baoding (N38.98, E116.10) and Dezhou (N37.35, E116.50). The first location is an urban site on top of a ~15m building, the second site is located in the countryside at the surface (~2m). During the campaigns four channel chemical speciation samplers (TH-16A Wuhan Tianhong Instruments Co., Ltd) containing two Teflon filters and two Quartz filters are used to collect measurement data including mass concentration, water soluble ionic (Cl^-, NO_3^-, SO_4^{2-}, Na^+, NH_4^+, K^+, Mg^{2+}, Ca^{2+}), element (Si, Na, Mg, Al, K, Mn, Fe, Ba, P, Ca, Ti, V, Cr, Co, Ni, Cu, Zn, As, Se, Mo, Cd, Tl, Pb, Th, U), OC and EC.

Satellite remote sensing data

Due to the limited availability of in-situ observations we have made use of remote sensing observations from satellites to put the modelled aerosol and precursor distributions in a larger perspective. The screening against satellite data focused on aerosol optical thickness (AOT) and two important precursors for the formation of particulate matter: NO_2 and NH_3.

The modelled aerosol distribution was compared to AOT observations from the MODIS satellite instrument. We used the MODIS collection 6 data (Levy and Hsu, 2015) from the AQUA satellite with local time overpasses at 13:30 UTC. The resolution of the

MODIS AOT product is 10x10 km^2. For each retrieval a simulated value was constructed matching the satellite pixel in time and position.

The NO_2 distribution is compared to tropospheric NO_2 columns retrieved from the OMI instrument with local overpass time at 13:30 UTC. We used the DOMINO version2.0 product (Boersma et al., 2011) which has a footprint of 13x24 km^2 at nadir. For each retrieval a simulated value was constructed matching the satellite pixel in time and position. The modelled NO_2 columns are further converted using the averaging kernels of the OMI observations, to take into account the sensitivity of the observation for NO_2 at different altitudes. Only retrievals with a cloud radiance fraction (fraction of radiance coming from the cloudy part of the pixel) lower than 50% are used.

Finally, we compare the modelled ammonia distributions to novel satellite retrieved ammonia columns from IASI as developed by (Van Damme et al., 2014a). Here we used the NH_3 vertical column densities (VCDs) retrieved from the IASI-A morning overpass observations (i.e. 09:30 Local Time) which have footprints between 12km x 12 km at nadir and up to 20 km x 39 km at the outermost angles. To select the observations with the highest quality we only use retrievals with a thermal contrast above 12 K and an relative error less than 100%. For each retrieval a simulated value was constructed matching the satellite pixel in time, position and shape following (Van Damme et al., 2014b). Although the satellite offers in principle daily coverage we compare the annual average modelled and retrieved ammonia VCD as the uncertainty in individual retrievals remains rather high. Unfortunately, dedicated evaluation of this product is hardly available. First evaluations using FTIR-instruments shows that the IASI-product may underestimate the actual ammonia columns by about 30% (Dammers et al., 2016).

Part I. Impact of updated emission inventories

I.1 Introduction

For this study we have compared model results using either the MEIC emission inventory or the MarcoPolo inventory. The runs have been performed for 2014, the year for which the MarcoPolo inventory has been made available. For the run using MEIC emissions we have used the MEIC emissions from 2010 as these were the most recent available to us. As some emissions have decreased and other have increased between 2010 and 2014, this may result in biases in the modelled fields when using the MEIC emissions.

I.2 Differences in emissions

MarcoPolo deliverable D.4.2 presents the produced MarcoPolo emission inventory and identifies the main differences between the MEIC 2012 and the MarcoPolo 2014 inventories. Below we have copied some plots from D4.2 highlighting these differences.

Focussing on the yearly total emissions in the domain, the largest deviations are observed for particulate matter. The PM2.5 and PM10 emissions differ by approximately 40%, with the larger value observed in the satellite based emissions. For nitrogen dioxide, the difference is approximately 25%, with lower totals for the satellite based emissions. For SO2 and VOC, both emission datasets differ at most 15%.

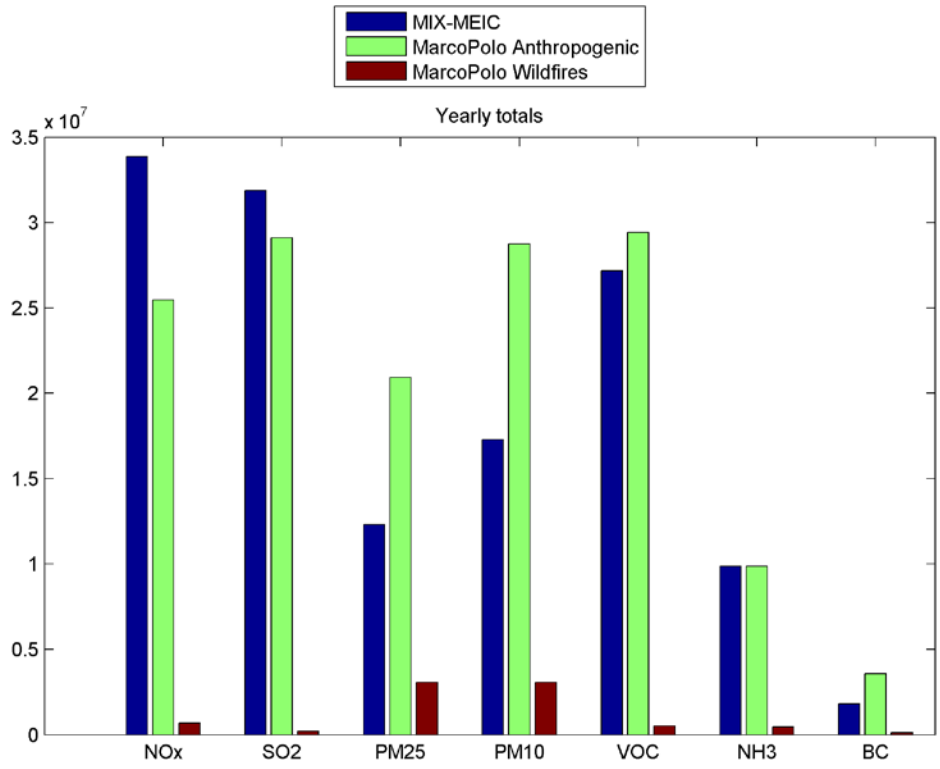

Figure 1 Comparison of the yearly total anthropogenic emissions contained in the MIX-MEIC 2012 inventory (blue) and the 2014 MarcoPolo low resolution inventory (green). Also the biogenic emissions in the MarcoPolo inventory are shown (dark red). For lay-out reasons, the results for CO are not shown. All emissions are provided in ton/year. (Figure taken from Deliverable 4.2)

Figure 2 shows the monthly profiles of the emissions. For PM2.5. the seasonal cycle in both emission inventories is similar. However the emissions in the MarcoPolo inventory are much higher than in the MEIC inventory for January and March, and much lower in February, July and September. For NOx emissions the seasonal cycle is very different in both inventories. However it should be noted that absolute differences are much smaller (up to 15%) than for PM2.5 (up to 30-40%). The updated inventory generally shows higher emissions in summer and lower in winter. For VOC emissions this is the other way around: updated emissions are higher in winter and lower in summer. The differences in VOC emissions are much larger (up to 40%) than in the NOx emissions. The changes in the updated SO2 emissions are small. Main feature is a ~7% decrease of the emissions in February. This decrease of emissions in February is visible in PM2.5, NOx and SO2.

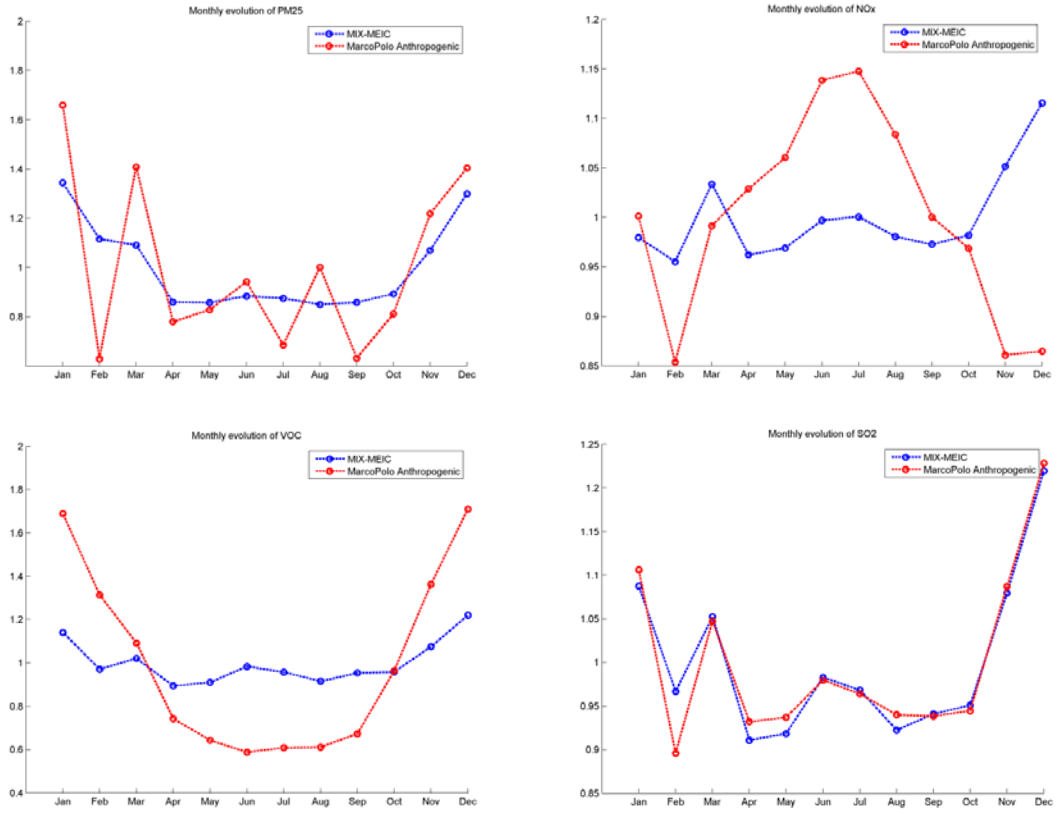

Figure 2 Monthly profiles of the four pollutants for which emissions are directly based on satellite estimates (top left: PM2.5, top right: NOx, bottom left: VOC, bottom right: SO2). For each pollutant, the figure shows the profile for the MIX-MEIC 2012 inventory (blue) and the anthropogenic emissions contained in the MarcoPolo 2014 low resolution inventory (red).

Figure 3 provides a comparison between the sector split of the total anthropogenic annual emissions contained in the MarcoPolo and the MIX-MEIC 2012 inventory. There are substantial differences in the source attribution of the total annual emissions. For particulate matter, the differences are rather small, but for the other pollutants there are major distinctions. In comparison with the MIX-MEIC 2012 inventory, the MarcoPolo inventory contains in general more residential emissions and less industrial emissions. The reason hereof is the different spatial distribution of the emissions, as the satellite based emissions are much more concentrated on large cities. This trade-off between the industrial and residential emissions is the largest for VOC, but it is also clearly existing for SO_2 and particulate matter, and, to a lesser extent, for nitrogen dioxide. Finally, the relative importance of transportation is much larger in the MarcoPolo inventory, in comparison with the MIX-MEIC 2012 inventory.

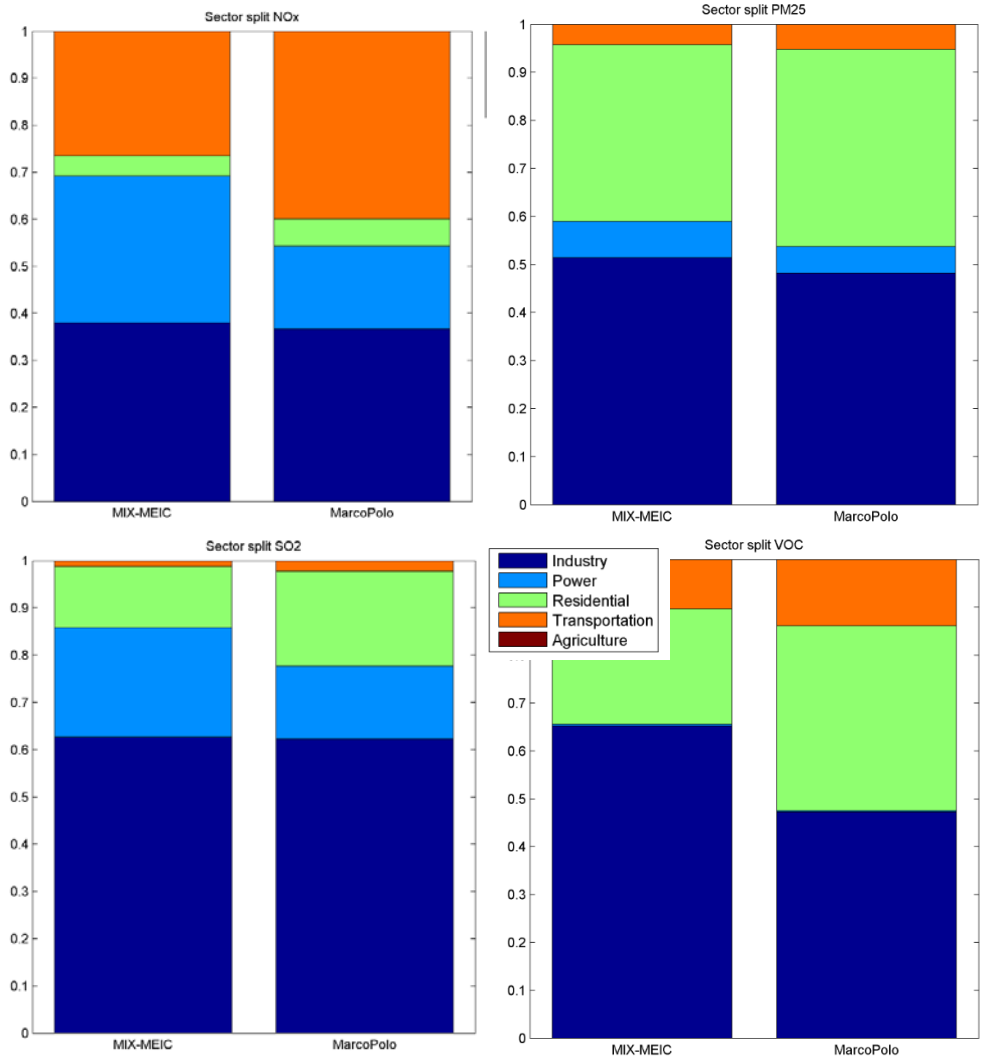

Figure 3 Comparison of the sector split of the yearly total emissions contained in the low resolution MarcoPolo emission inventory (right) and the MIX-MEIC 2012 inventory (left), for the five sectors contained in both inventories (from bottom to top: industry, power, residential, transportation and agriculture). Results are shown for NOx (top left), PM2.5 (top right), SO2 (bottom left) and VOC (bottom right).

Figure 4 shows the distribution of yearly NOx and PM2.5 emissions for the two inventories. It is clear that the PM2.5 emissions are much higher in the MarcoPolo inventory over all source regions. For NOx we see lower emissions in the MarcoPolo inventory, especially near the Shanghai area, but also in the background area between Beijing and Shanghai.

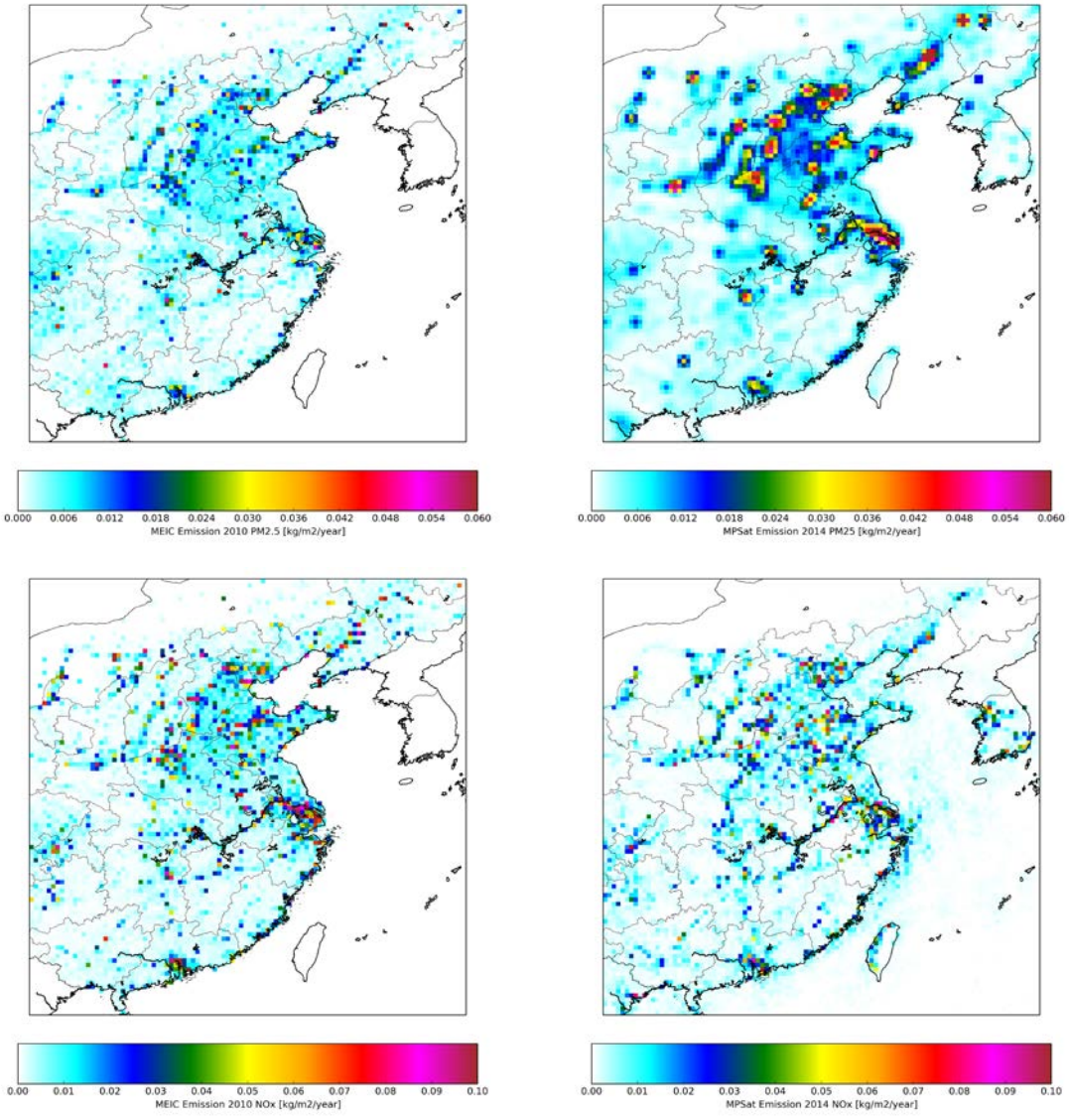

Figure 4 Distribution of yearly total PM2.5 (upper plots) and NOx emissions (lower plots) from the MEIC (left) and MarcoPolo (right) inventory.

I.3 Impact on modelled NO_2

We first evaluate the impact of the updated emissions by comparing the modelled fields with tropospheric NO_2 column fields from the OMI satellite instrument. Figure 5 shows that the yearly average modelled NO2 columns are smaller with the updated emissions which agrees with the 25% lower total emissions for NOx. While generally the model was overestimating the NO_2 columns in central and Northern China, with the updated emissions the model is now underestimating the NO_2 columns, especially around Beijing. The large overestimation over Shanghai is strongly decreased to values comparable to OMI. The underestimations of the model over some hotspots along the yellow river are not removed with the updated emissions.

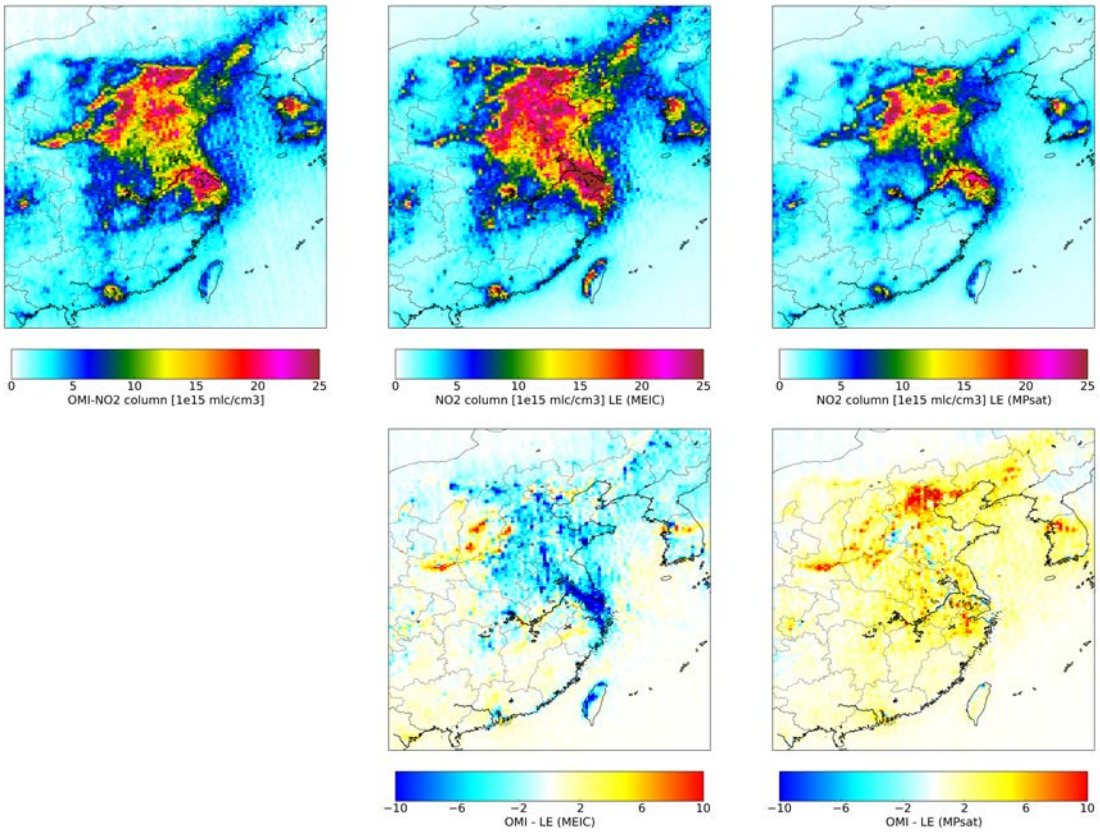

Figure 5 Yearly averaged tropospheric NO_2 columns from OMI satellite observations (left), colocated model values with MEIC emissions (middle) and colocated model values with MarcoPolo emissions (right) and observations minus model values (bottom row, in 1e15 mlc/cm3)).

Figure 6 and Figure 7 show a scatterplot and a monthly comparison for the Beijing and Shanghai areas. As mentioned before for Beijing the initial overestimation by the model is turned to a large underestimation with the updated emissions. For Shanghai however the updated emissions lead to an improved absolute agreement with the OMI data. The seasonal patterns are not largely altered over these areas despite the change in seasonal pattern visible in the average emissions over the entire country from Figure 2. Over both

areas the MarcoPolo emissions seem to miss the increase at the end of the year which is visible when using the MEIC emissions.

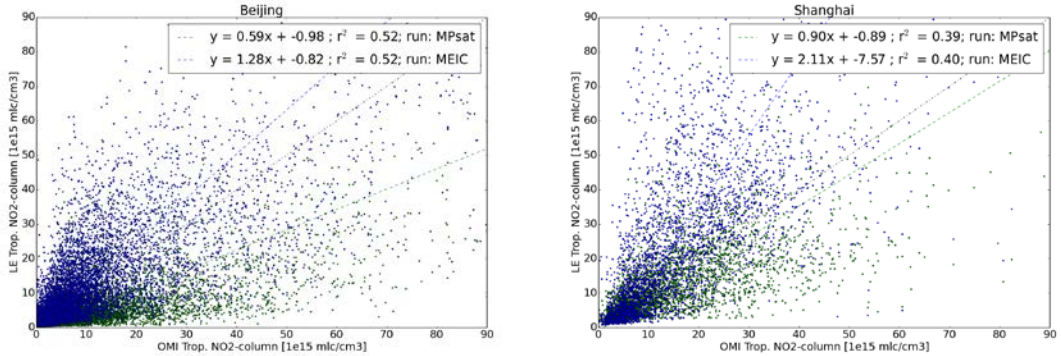

Figure 6 Scatterplot of modelled tropospheric NO_2 columns versus OMI satellite observations for the province of Beijing and Shanghai in 2014. In blue and green the model results using the MEIC and MarcoPolo inventory respectively.

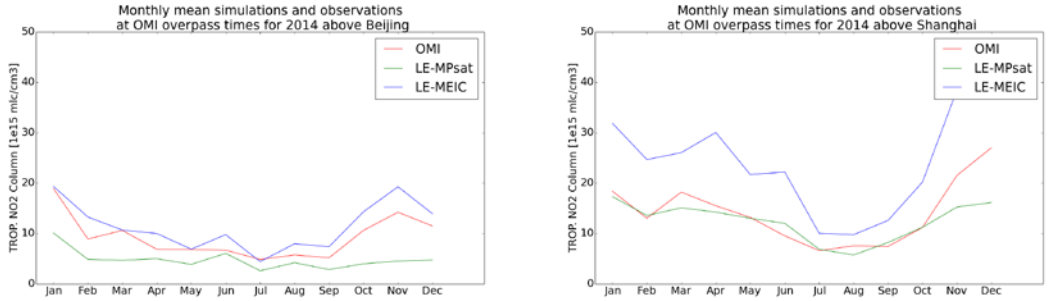

Figure 7 Timeseries of monthly mean NO_2 columns from OMI (red) and collocated model values from LOTOS-EUROS model with MEIC (blue) and MarcoPolo (green) emissions for Beijing and Shanghai in 2014.

Because the OMI tropospheric NO2 columns have been used in the emission inversion, the evaluation based on OMI data is not fully independent. To have a more independent evaluation we have also compared the model results to groundbased observations from the Shanghai environmental Monitoring Center (SEMC) in Shanghai and IAP in Beijing (Figure 8).While we have seen a large decrease in the modelled tropospheric NO_2 columns, the surface concentrations in both cities have increased. This may be due to the change in sector split in the emissions. The increased contribution of traffic emissions at the surface can counteract the decrease in total emissions which for different source sectors are attributed to higher levels (100-500 m for power sector and industry). On average the results from the run with MarcoPolo emissions are closer to the observed concentrations. In the first few months the satellite based emission inventory leads to higher NO_2 concentrations that are much closer to the observed high concentrations, however in the last part of the year the produced MarcoPolo inventory does not lead to a similar improvement.

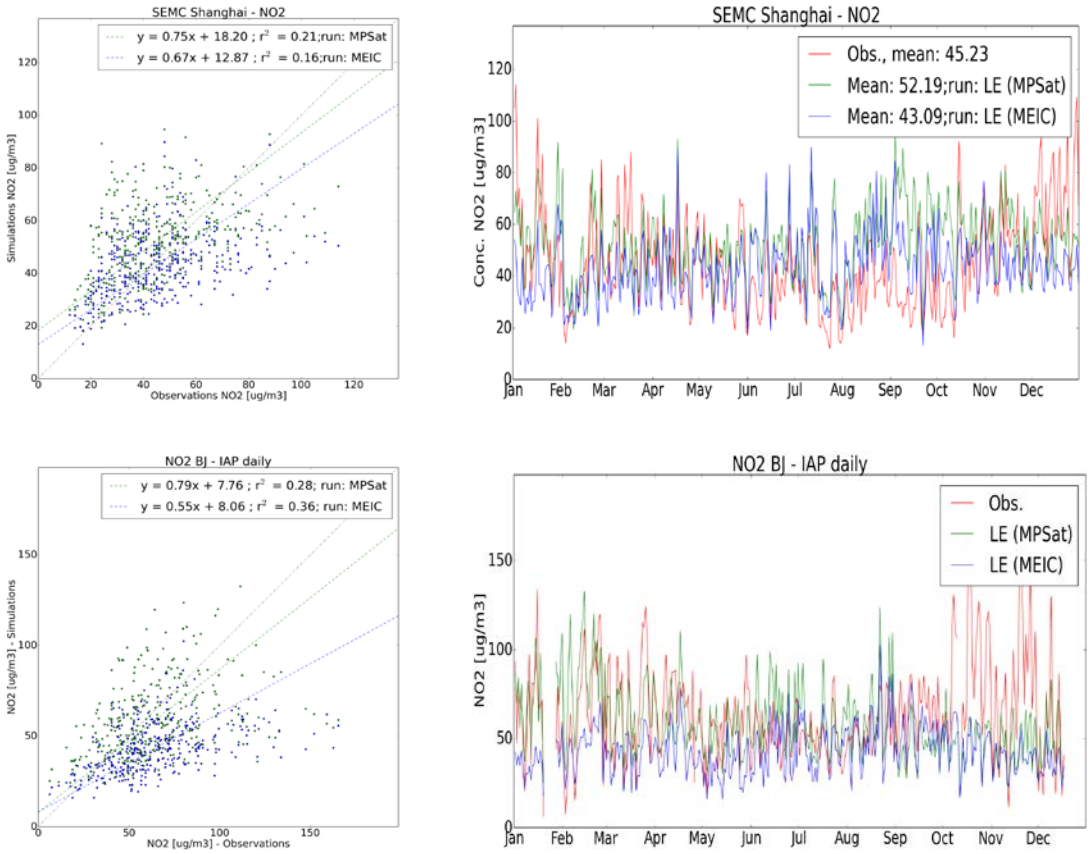

Figure 8 Scatterplot and timeseries from modelled daily surface NO2 versus surface observations from the SEMC in Shanghai and IAP in Beijing. In blue and green the model results using the MEIC and MarcoPolo inventory respectively.

IAP also provides observations for the cities of Tianjin, Shiazhuang, Chengde, and Qinhuangdao. Figure 9 shows the seasonal cycles for Beijing and the other 4 cities provided by IAP and modelled by LOTOS-EUROS. While the improvement from using the MarcoPolo emissions is clear in the first half of the year in Beijing. This improvement is not seen for the other stations. The strong increase of concentrations in winter in Tianjin, Shiazhuang and Chengde is not reproduced by the model with neither emission inventory. We know that many chemistry transport models have difficulty in reproducing the build-up of high concentrations in stable weather conditions with low boundary layers (Stern et al., 2008).

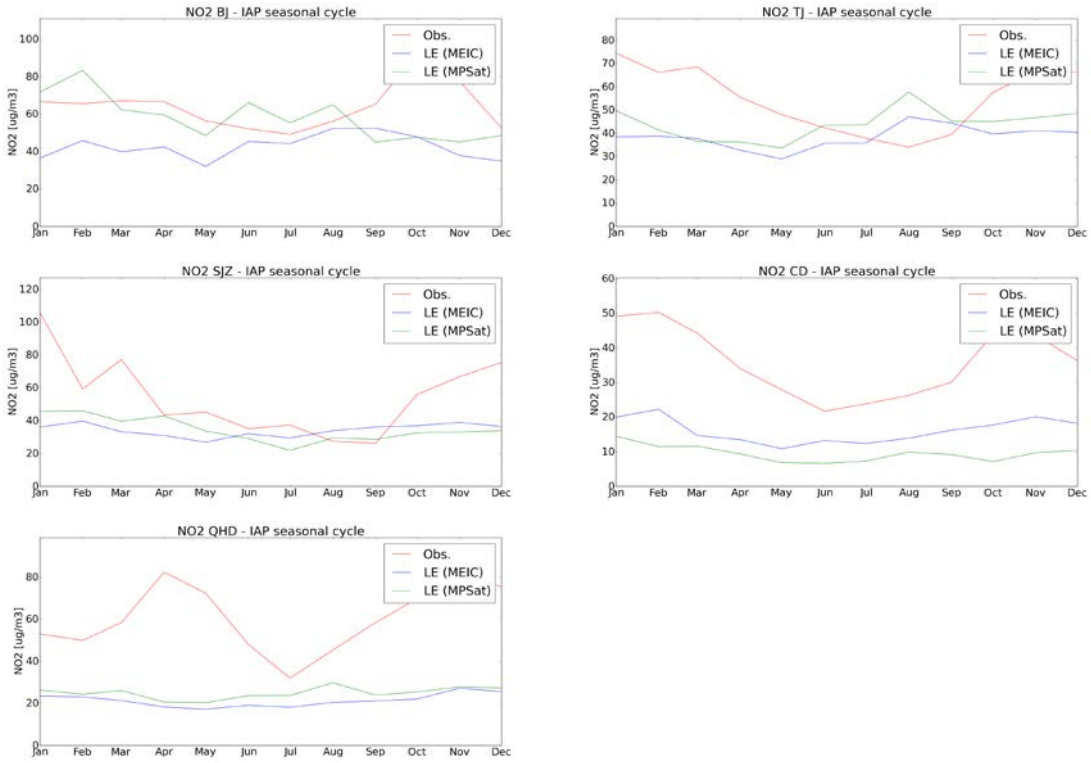

Figure 9 Modelled monthly surface NO2 versus IAP surface observation (red line) in Beijing (BJ), Tianjin (TJ), Shiazhuang (SJZ), Chengde (CD), and Qinhuangdao (QHD). In blue and green the model results using the MEIC and MarcoPolo inventory respectively.

I.4 Impact on modelled SO_2

The SEMC and IAP institutes also provide surface observations of SO_2 from the same stations as for NO_2. While the country total annual SO_2 emissions do not differ substantially, we do see some higher SO_2 concentrations over Shanghai and lower SO_2 concentrations over Beijing modelled with the MarcoPolo emissions (Figure 10). This can be due to regional changes in emissions or changes in the split over different source categories. Also changes in emissions of other constituents can lead to changes in SO_2 concentrations through chemical reactions.

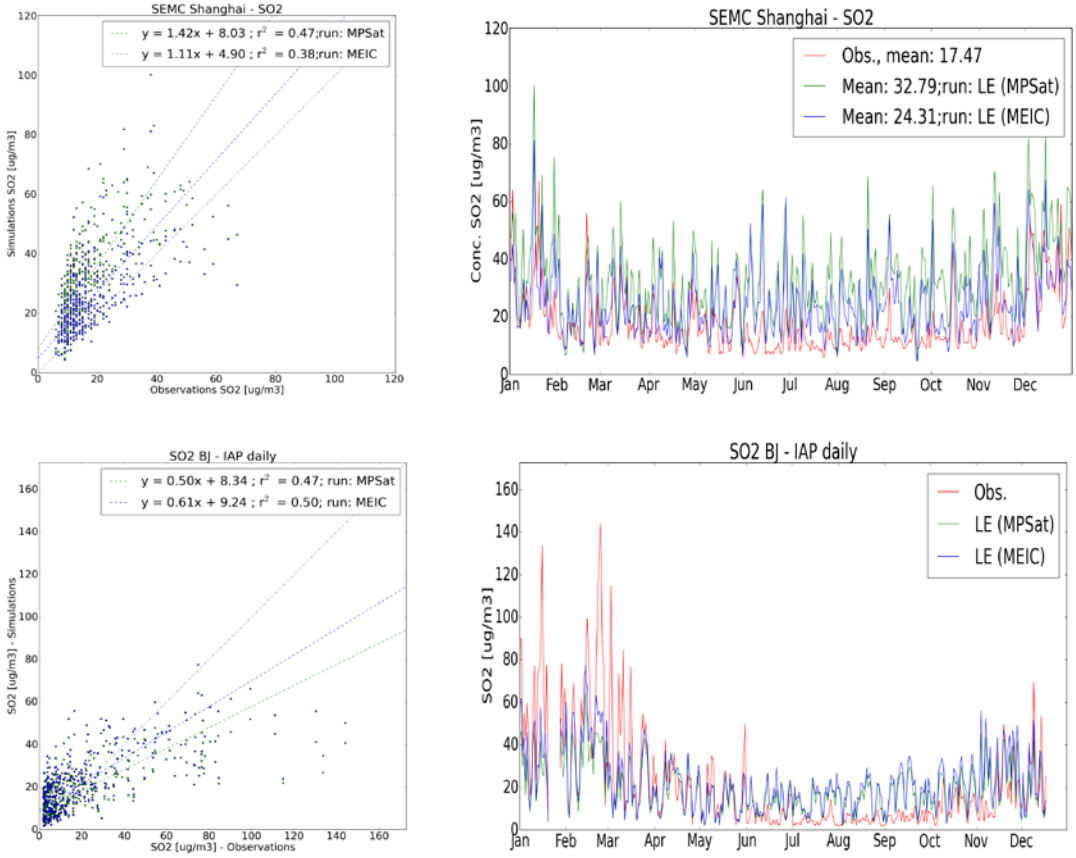

Figure 10 Scatterplot and timeseries from modelled surface SO_2 versus surface observations from the Shanghai environmental Monitoring Center (SEMC) in Shanghai and Institute of Atmospheric Physics (IAP) in Beijing. In blue and green the model results using the MEIC and MarcoPolo inventory respectively.

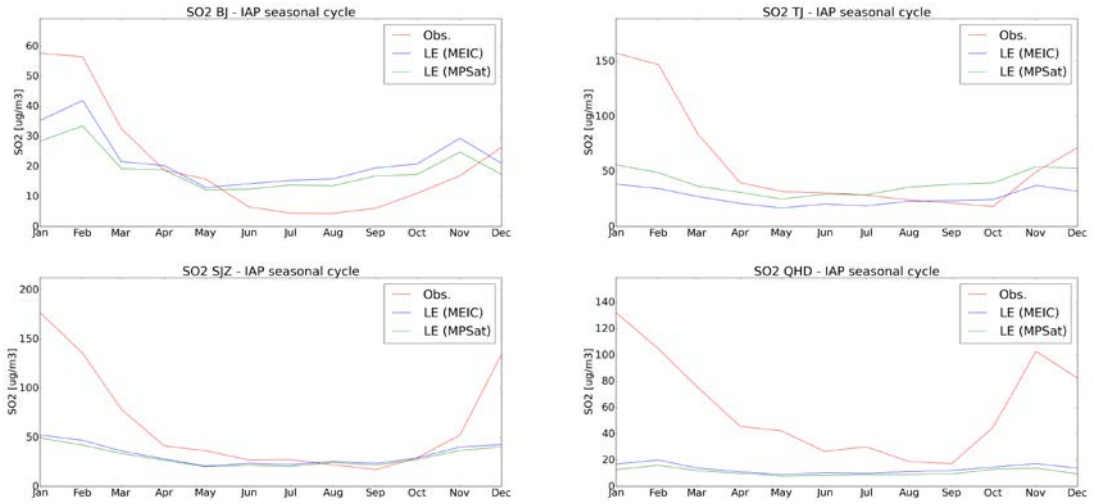

Figure 11 Modelled monthly surface SO2 versus IAP surface observation (red line) in Beijing (BJ), Tianjin (TJ), Shiazhuang (SJZ), and Qinhuangdao (QHD). In blue and green the model results using the MEIC and MarcoPolo inventory respectively.

Figure 11 shows the seasonal cycles for Beijing and 3 other cities provided by IAP and modelled by LOTOS-EUROS. The differences between both model runs are generally small and it's hard to draw any conclusions on the best performance. Again the underestimation of winter built-up of concentrations is clearly visible. The altitude at which the emissions are inserted in the model also can play a crucial role here. We performed a test run with altered vertical emission profiles, where more emissions are inserted at lower altitudes in the model. Figure 12 shows the large influence of using a different vertical emission profile. Although the comparison with observations with the new profiles improves in winter, it also leads to an overestimation from spring onwards. More knowledge on the altitude of the emissions from different sources is required to allow better performances of the model.

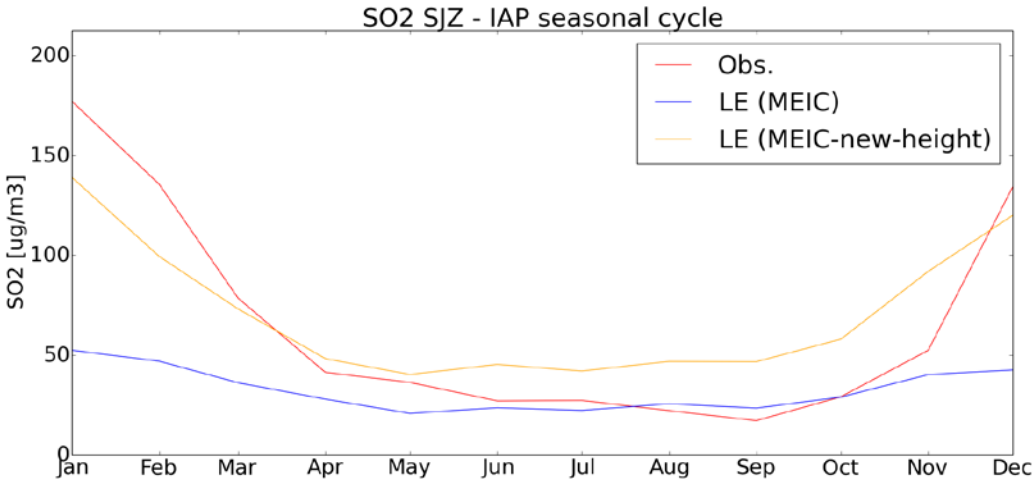

Figure 12 Monthly surface SO2 versus IAP surface observation (red line) in Shiazhuang (SJZ). In blue and yellow the model results using the standard and altered vertical emission profiles respectively.

I.5 Impact on modelled aerosols

We first evaluate the impact of the updated emissions by comparing the modelled fields with AOT columns from the MODIS satellite instrument. Figure 13 shows that the yearly average modelled AOT columns are higher with the updated emissions which agrees with the ~40% increase total emissions for PM. While the model was showing a substantial underestimation over the areas with highest AOT values with the MEIC emissions as input, the model is showing agreement and overestimation of the yearly average AOT when using the MarcoPolo emission inventory.

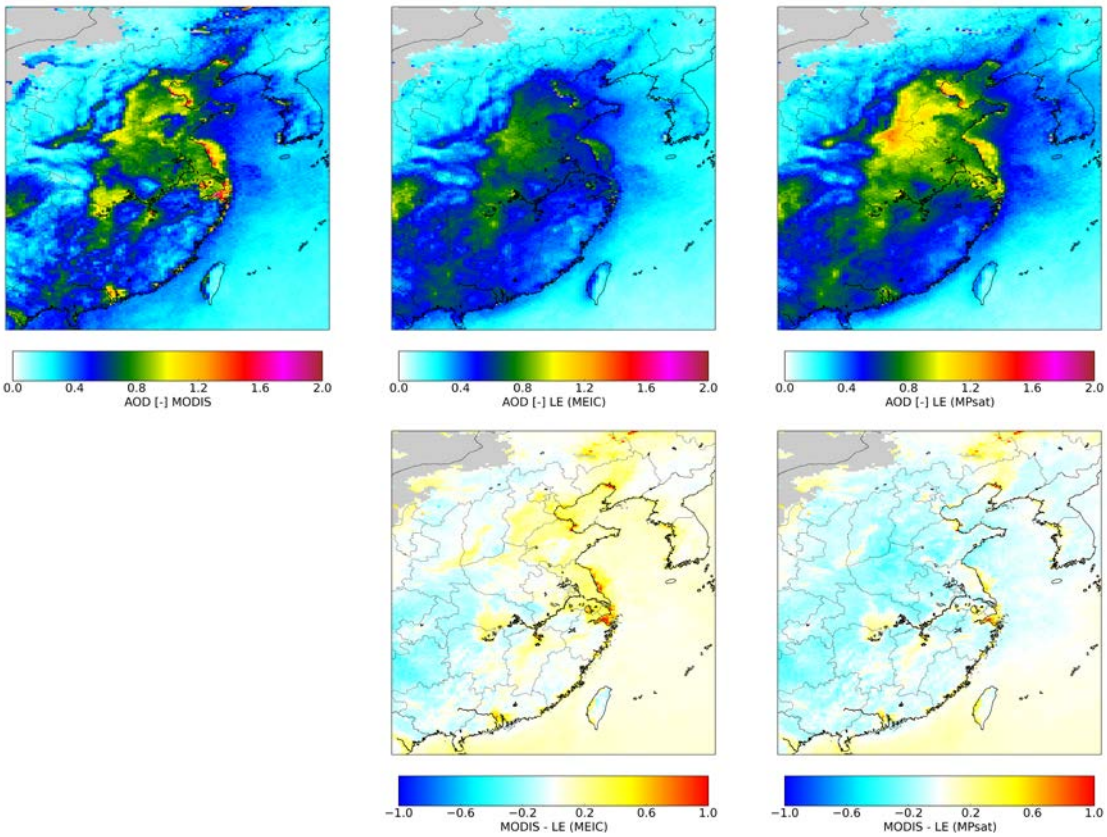

Figure 13 Yearly averaged AOT columns from MODIS satellite observations (left) model with MEIC emissions (middle) and model with MarcoPolo emissions (right) and observations minus model values (bottom row).

Figure 14 and Figure 15 show a scatterplot and a monthly comparison for the Beijing, Shanghai, Shijazhuang and Tianjin areas. On average the agreement with MODIS observations is much better when using the MarcoPolo inventory. The correlation coefficient is slightly better when using the MEIC inventory. The seasonal patterns do not change much when using the MarcoPolo inventory, except for the peaks of emissions in January for all 4 sites and in March for Shijazhuang and Shanghai. Except for Shanghai this leads to a large overestimation of the AOT in January. As we know we are missing aerosols

in the model (e.g. no secondary organic aerosols (SOA), resuspended dust), thus an overestimation of aerosol values is not expected.

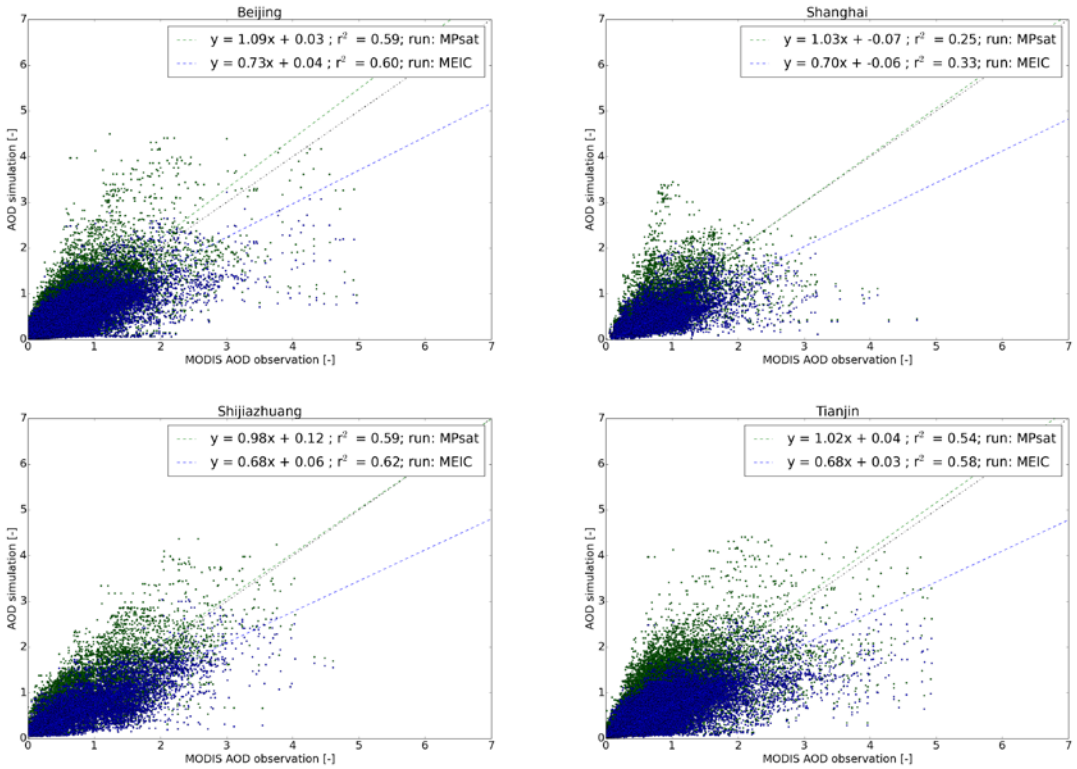

Figure 14 Scatterplot of modelled tropospheric AOT columns versus MODIS satellite observations for the province of Beijing, Shanghai, Shijazhuang and Tianjin in 2014. In blue and green the model results using the MEIC and MarcoPolo inventory respectively.

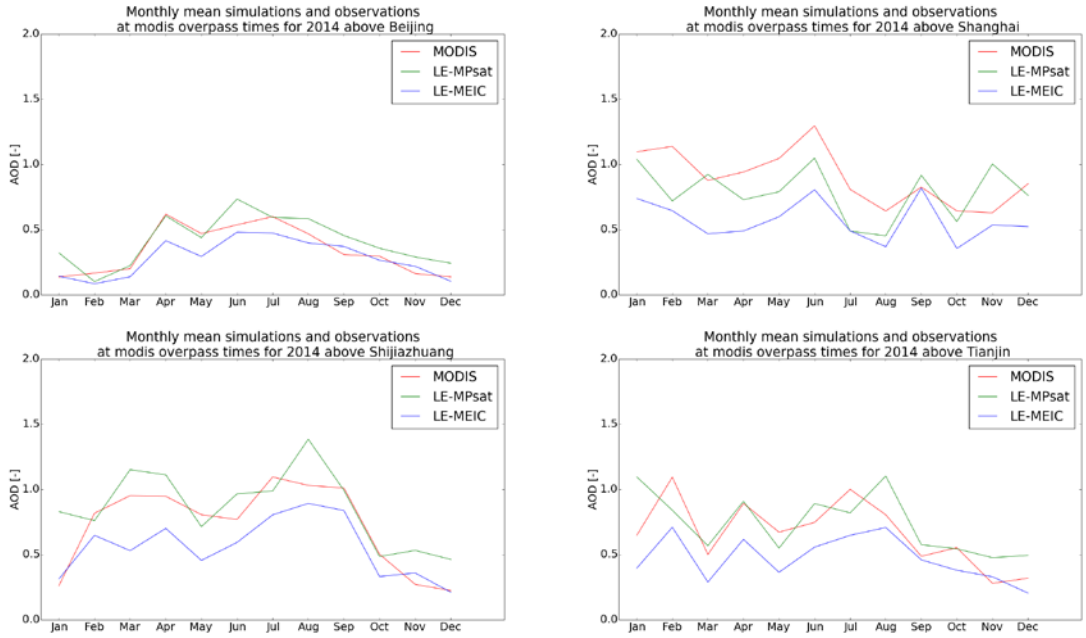

Figure 15 Timeseries of monthly mean AOT columns from MODIS (red) and collocated model values from LOTOS-EUROS model with MEIC (blue) and MarcoPolo (green) emissions for Beijing, Shanghai, Shijazhuang and Tianjin in 2014.

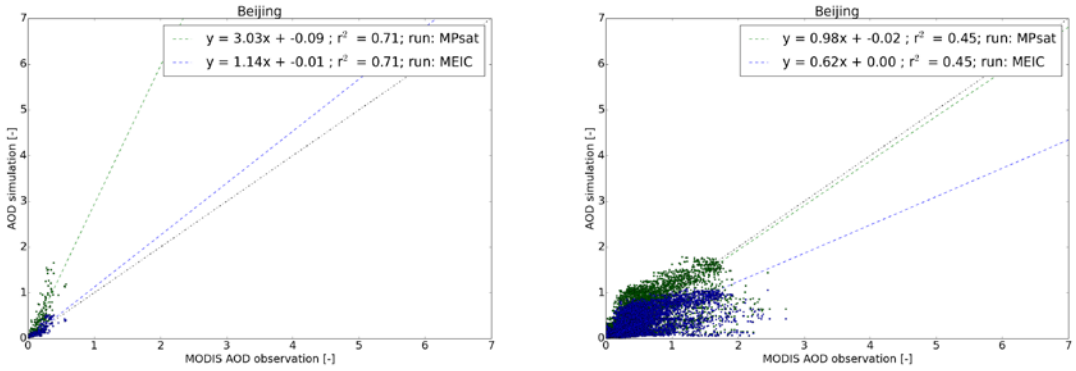

Figure 16 Scatterplot of modelled tropospheric AOT columns versus MODIS satellite observations for the province of Beijing for January (left) and May (right) 2014. In blue and green the model results using the MEIC and MarcoPolo inventory respectively.

In general the model run with MarcoPolo emissions seem to have better agreement with MODIS AOT observations in the spring and summer period, but a very large overestimation in the winter months January and December. This high overestimation can also be seen in scatter plot for January in comparison to a very nice agreement in e.g. May (Figure 16).

Again we have also compared our results with independent groundbased observations.

The comparison with observations from SEMC and IAP in Figure 17 shows that the underestimation when using MEIC emissions is replaced by an overestimation when using the MarcoPolo inventory. From the timeseries we can conclude that the overestimation is mainly present during some specific months.
The same conclusion can be drawn from the comparison to US embassy PM2.5 data in Shanghai, Beijing, Guangzhou and Shenyang (Figure 18 and Figure 19). For Guangzhou the comparison looks reasonable with only small differences from using different emission sets but for the other locations some extreme overestimations of observed concentration occur with values of up to 2000 µg/m^3 in January in Beijing when using the MarcoPolo inventory. It seems that the emission inversion is hampered by e.g. high altitude dust aerosols during some months of the years, while for other months the emission inversion is providing more realistic emission data. It can be possible that high AOT values due to dust aerosols are attributed to local surface emission sources, leading to overestimated emissions and resulting modelled concentrations at the surface.

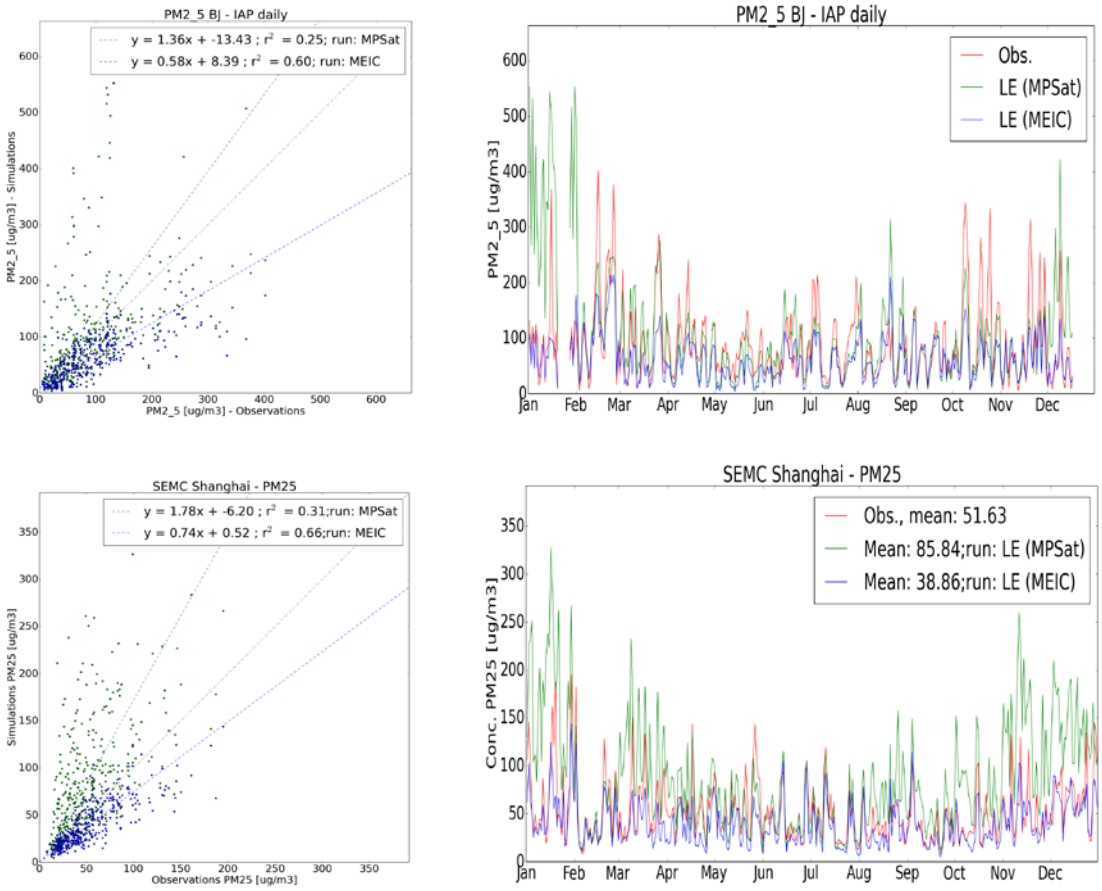

Figure 17 Scatterplot and timeseries from modelled surface PM2.5 versus surface observations from the Institute of Atmospheric Physics (IAP) in Beijing (upper plots) and Shanghai environmental Monitoring Center (SEMC) in Shanghai (lower plots). In blue and green the model results using the MEIC and MarcoPolo inventory respectively.

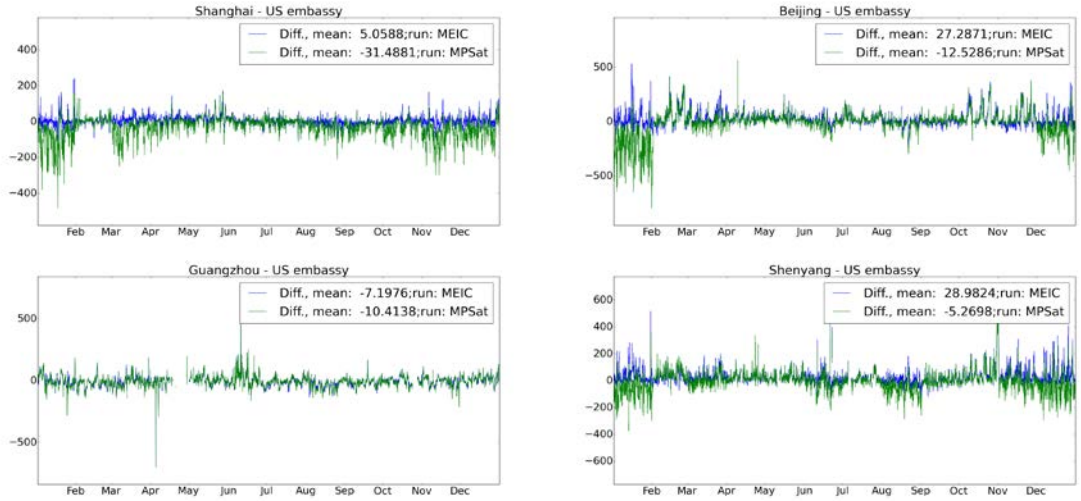

Figure 18 Timeseries of observation minus modelled surface PM2.5 in Shanghai, Beijing, Guangzhou and Shenyang. In blue and green the model results using the MEIC and MarcoPolo inventory respectively.

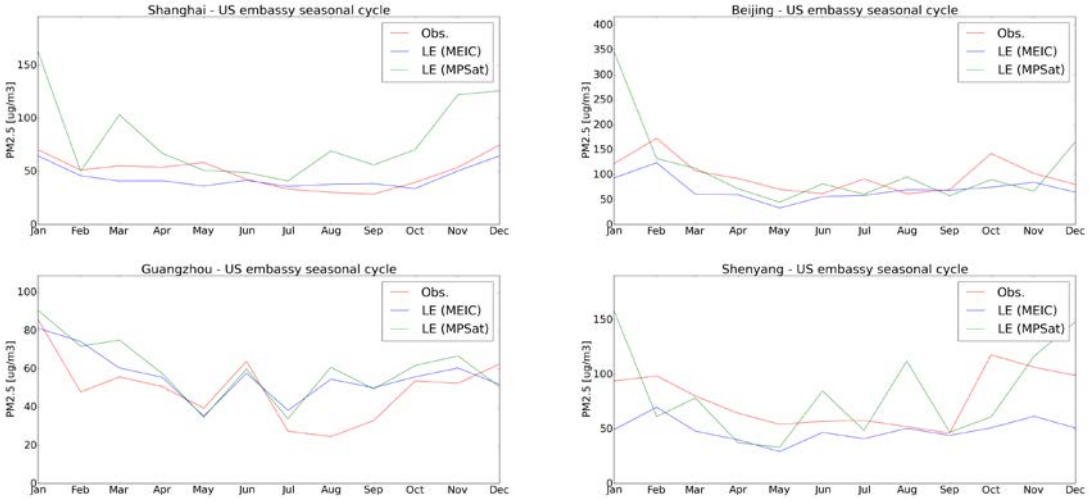

Figure 19 Monthly timeseries of surface PM2.5 from US embassy stations (red) and from the LOTOS-EUROS model in Shanghai, Beijing, Guangzhou and Shenyang. In blue and green the model results using the MEIC and MarcoPolo inventory respectively.

I.6 Conclusion impact updated emissions

The updated emission inventory from MarcoPolo seems to produce realistic results for NO_2 and SO_2. While the updated emissions lead to lower NO_2 columns and better agreement with OMI satellite data, the impact at the surface in most cases is an increase of NO_2 as the source splits are changed. For the first part of 2014 over Beijing the updated emissions lead to better agreement with observations however, the updated emissions do not lead to a consistent improvement over all regions and seasons.

For PM, it seems that the emission inventory contains too large PM emissions for certain months of the years, over certain regions within China. For example in January over Beijing these updated emissions lead to overestimation of surface PM2.5 with up to 2000 $\mu g/m^3$. Because of these large discrepancies the use of the updated PM emission inventory is not recommended until issues have been resolved and an update of the inventory has taken place.
To this end the source apportionment of PM over China which is discussed in part II, is based on the MEIC emission inventory.

Part II. PM source apportionment over China

II.1 Source apportionment set-up

LOTOS-EUROS includes a source apportionment technique to track the origin of particulate matter components and its precursor gases (Kranenburg et al., 2013). This module uses a tagging approach similar to the approach taken by Wagstrom et al. (2008), tracking the contribution of a predefined set of emission categories through the model simulation. For reactive components the preserved atoms of N, S, and C are tracked through the chemistry. The labels can be defined flexibly discriminating e.g. countries/provinces, sectors or fuel type. Hence, besides the concentration of each tracer also the corresponding fractional contribution of each label is calculated. For details and validation of this source apportionment module we refer to Kranenburg et al. (2013). Previous applications to particulate matter and its precursors are documented in Banzhaf et al. (2015), Hendriks et al. (2016, 2013) and Schaap et al. (2013).

The model was ran for the year 2013 using ECMWF meteorological data to drive the model. Through a one-way nesting procedure a simulation over East-China was performed on a resolution of 0.25° longitude by 0.125° latitude, approximately 21 by 15 km^2. This domain (see Figure 21) is nested in a larger domain covering China almost entirely with a resolution 1° longitude by 0.5° latitude, approximately 84 by 56 km^2. Chemical boundary conditions for the coarse resolution domain were taken from the MACC global modelling framework (Flemming et al., 2009). Here we study the origin of PM in terms of area as well as source sector. We have tracked the 5 main source categories as well as the emissions from Beijing and Shanghai. To be able to assess the contributions of the regions around the cities the larger areas Tianjin-Hebei (TH), Yangtze River Delta and Pearl River Delta were labelled separately (see Figure 21). This resulted in 35 labels, including labels for natural emissions such as desert dust and sea-salt and for influx from outside the model domain. The labels are listed in Table 1.

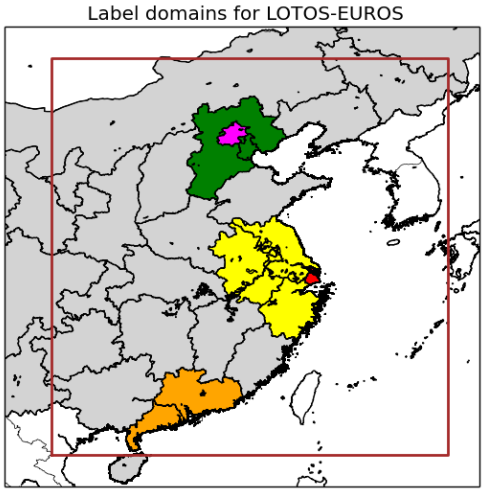

Figure 20. Map of high resolution run domain (red square) and label domains (Pink = Beijing, Green = Tianjin-Hebei, Red= Shanghai, Yellow = Yangtze river delta, Orange = Pearl River Delta).

Table 1. Overview of labels applied in the source apportionment run

Labelled domains
Beijing – 5 source sectors
Tianjin-Hebei – 5 source sectors
Shanghai – 5 source sectors
Yangtze River delta – 5 source sectors
Pearl River delta – 5 source sectors
Rest of China – 5 source sectors
Outside China – no sector division
Natural (sea salt, desert dust, forest fires)
Outside model domain – (lateral boundary, top boundary, initial model condition)

5 Source Sectors
Energy
Residential combustion
Industry
Transport
Agriculture

II.2 Validation of concentration fields

The source apportionment was performed for the year 2013, which is different from the year 2014 for which the impact of updated emissions was made. The modelled concentrations of PM and its precursors for 2013 have been validated with both satellite and surface observations . For a detailed description of validation results we refer to (Timmermans et al., 2016). The main conclusion is that the model is able to capture the day to day variability in PM2.5 as induced by synoptic meteorology. The model is however underestimating the PM levels, with largest underestimations in the winter period, as can be seen in Figure 22. The underestimation is attributed to:

- Underestimation of residential combustion due to additional heating in the winter
- Uncertainties in dust emissions from desert areas as well as dust AOT calculations.
- Resuspension of dust due to traffic and other anthropogenic activities which is not taken into account in the model.
- SOA formation which is not included in this model version
- Reduction of radiation in very polluted situations
- Difficulties in modeling air pollutant build up in very stable weather conditions
- Increased heterogeneous chemistry during haze, not taken into account in the model.

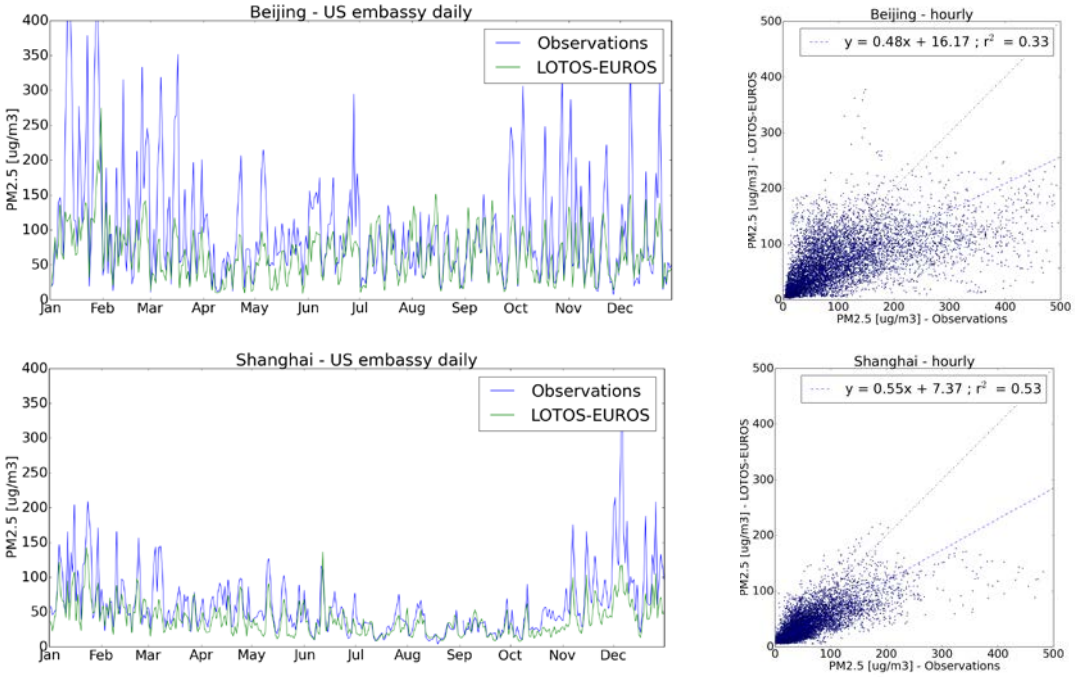

Figure 21 Comparison of LOTOS-EUROS (red line) daily PM2.5 with in-situ observations (blue line) from the US embassy stations at Beijing (top) and Shanghai (bottom) in 2013

These conclusions are supported by the comparison to the PM composition data from Peking university obtained during two campaigns in 2013 at the sites of Baoding and Dezhou. The statistical comparison of modelled values with these observations shows that the winter underestimation, which is especially large in Baoding, is partly due to missing organic aerosols in the model. But the gap in PM2.5 can not be filled with the gap in OM or other observed components. It is also clear that the high PM levels are not solely due to the observed components listed in the table, but also due to non observed components such as primary PM2.5 and dust.

Table 2 Statistical comparison of simulated aerosol concentrations and speciated observations from Peking University.

	Dezhou		Baoding		Dezhou		Baoding	
	summer	winter	summer	winter	summer	winter	summer	winter
	PM2.5				NO3			
observation	73.6	169.7	74.5	223.6	12.0	23.8	11.2	20.6
simulation	56.3	61.4	59.2	56.0	18.3	12.6	18.5	8.7
bias	-17.3	-108.4	-15.2	-167.6	6.3	-11.2	7.3	-11.9
relative bias	-23.5	-63.8	-20.4	-75.0	52.9	-46.9	65.3	-57.6
	EC				SO4			
observation	1.7	4.1	2.8	6.1	24.5	24.5	20.1	18.4
simulation	2.1	5.4	2.6	5.6	10.6	2.4	10.0	1.8
bias	0.5	1.3	-0.2	-0.5	-13.9	-22.1	-10.0	-16.5
relative bias	27.5	32.2	-8.0	-7.9	-56.7	-90.3	-50.0	-90.0
	OM/POM				NH4			
observation	6.2	41.1	11.5	74.0	12.2	17.5	9.7	15.7
simulation	3.0	10.0	3.8	10.5	9.2	4.6	9.1	3.2
bias	-3.2	-31.1	-7.8	-63.5	-3.0	-13.0	-0.6	-12.4
relative bias	-51.3	-75.6	-67.3	-85.8	-24.2	-74.0	-6.1	-79.4

The PM2.5 source apportionment provided below therefore provides a best estimate using currently available LOTOS-EUROS modelling techniques and emission information, albeit only for the modelled fraction. In the future, time series of PM composition needs to be evaluated in detail to better assess the performance of the model system.

II.3 Source apportionment results

Table 3 shows the 2013 yearly averaged contributions to modeled PM2.5 and PM10 for the grid cells located over the center of Beijing and Shanghai. About half of the modeled PM2.5 is coming from the municipality itself. For PM10, the local contribution is slightly lower due to the contribution from the natural sources: dust and sea salt. About a quarter of

the PM2.5 comes from the surrounding provinces and the remaining quarter comes from long range transport and natural sources. Our estimate of the local contribution is at the lower range of available studies. Other model studies directed at Beijing and Shanghai found contributions of 52-72% of the city itself (Lang et al., 2013; Li et al., 2015; Zhang et al., 2015). An overview of source apportionment results released by five different cities (Beijing, Tianjin, Shijiazhuang, Jinan and Shanghai) indicate local contributions between 64 and 84% (Wei et al., 2015). The main source of PM 2.5 in Beijing is residential combustion, additional large source contributions from industry and transport are present. In Shanghai the largest contribution to PM2.5 is from industry, also residential combustion and transport contribute substantially to the yearly average PM2.5.

Table 3 Source category and area contributions (in %) to total PM2.5 and PM10 in Beijing and Shanghai in 2013.

	Beijing				Shanghai			
	Local	Regional	Long range transport	Total	Local	Regional	Long range transport	Total
PM2.5	49.2	25.7	21.1	100.0	44.6	24.7	24.3	100.0
Power sector	0.7	2.2	4.6	7.5	2.3	4.3	4.1	10.7
Residential combustion	20.4	8.2	4.6	33.2	9.4	5.2	6.8	21.4
Industry	6.8	9.7	8.6	25.0	14.7	9.9	9.8	34.4
Transport	19.4	3.3	1.8	24.4	14.7	3.0	2.2	19.9
Agriculture	2.0	2.4	1.5	5.9	3.4	2.3	1.5	7.2
Natural	-	-	-	1.7	-	-	-	2.3
Outside China	-	-	-	2.4	-	-	-	4.2
PM10	42.5	22.8	19.0	100.0	38.7	22.9	22.0	100.0
Power sector	0.6	1.9	4.0	6.5	2.3	4.1	3.7	10.1
Residential combustion	18.1	6.9	4.0	28.9	8.1	4.1	5.5	17.7
Industry	7.4	9.8	8.5	25.7	14.6	10.7	9.8	35.1
Transport	14.9	2.5	1.4	18.7	11.1	2.4	1.9	15.4
Agriculture	1.5	1.8	1.1	4.4	2.5	1.7	1.1	5.4
Natural	-	-	-	13.9	-	-	-	12.6
Outside China	-	-	-	1.9	-	-	-	3.9

Figure 24 and Figure 25 show the seasonal dependence of the source contributions. It is clear that residential combustion has a larger contribution during the cold seasons, when shallow mixing layers and additional heating during cold spells lead to high concentrations of PM. This is especially visible in the first three months over Beijing, where about 60% of the PM2.5 is coming from local residential combustion sources. During the summer the main sources are industry and transport.

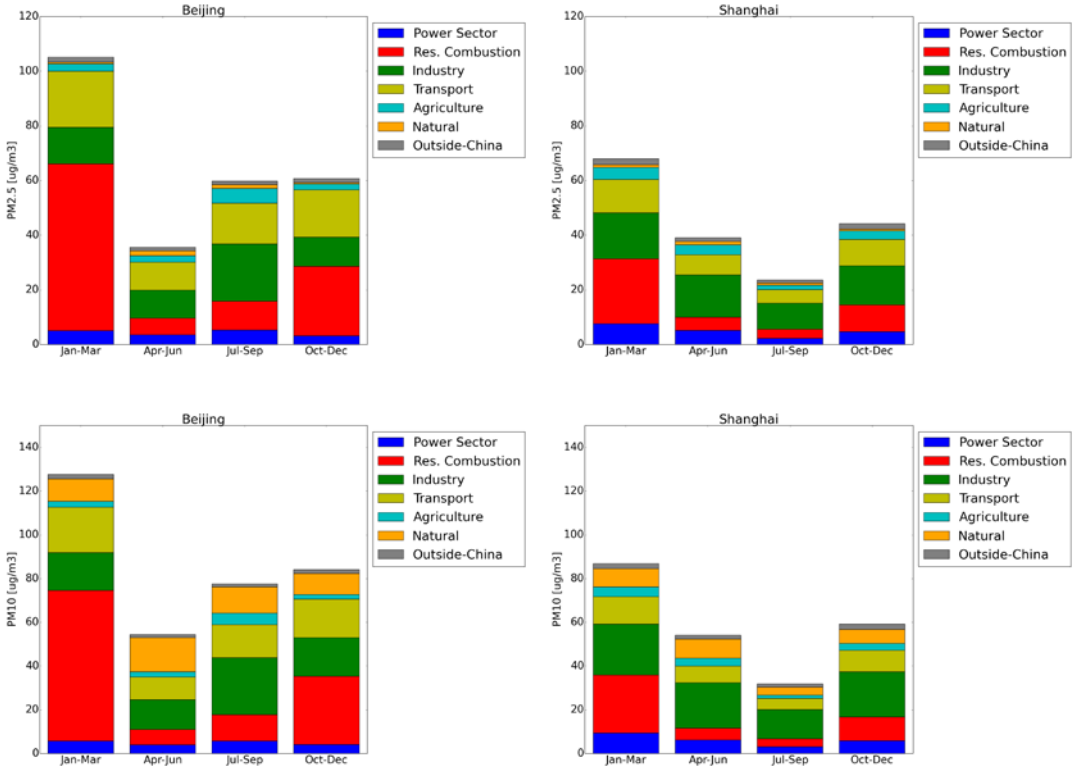

Figure 22 Dominant source categories for PM2.5 (upper plots) and PM10 (lower plots) for different seasons in Beijing (left column) and Shanghai (right column).

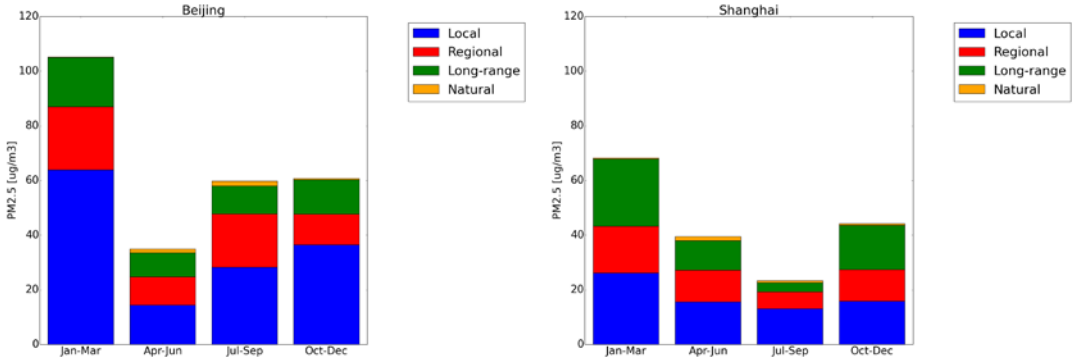

Figure 23 Dominant source regions for PM2.5 for different seasons in Beijing (left) and Shanghai (right).

To investigate the origin of particulate matter at high episodic concentrations the origin and composition is provided as a function of the modelled PM2.5 concentrations (Figure 25). In general, the relative contribution of especially nitrate increases with increasing PM2.5 concentrations, which matches well with experimental data from e.g. Huang et al. (2014) and modelling results from Hu et al. (2016). The increasing share of secondary material

explains the increasing share of contributions from outside the cities with increasing PM2.5 levels. In contrast to Shanghai the results for Beijing show a slight increase of the local contribution at the highest end of the range which is attributed to the contribution from residential combustion, which shows the same pattern.

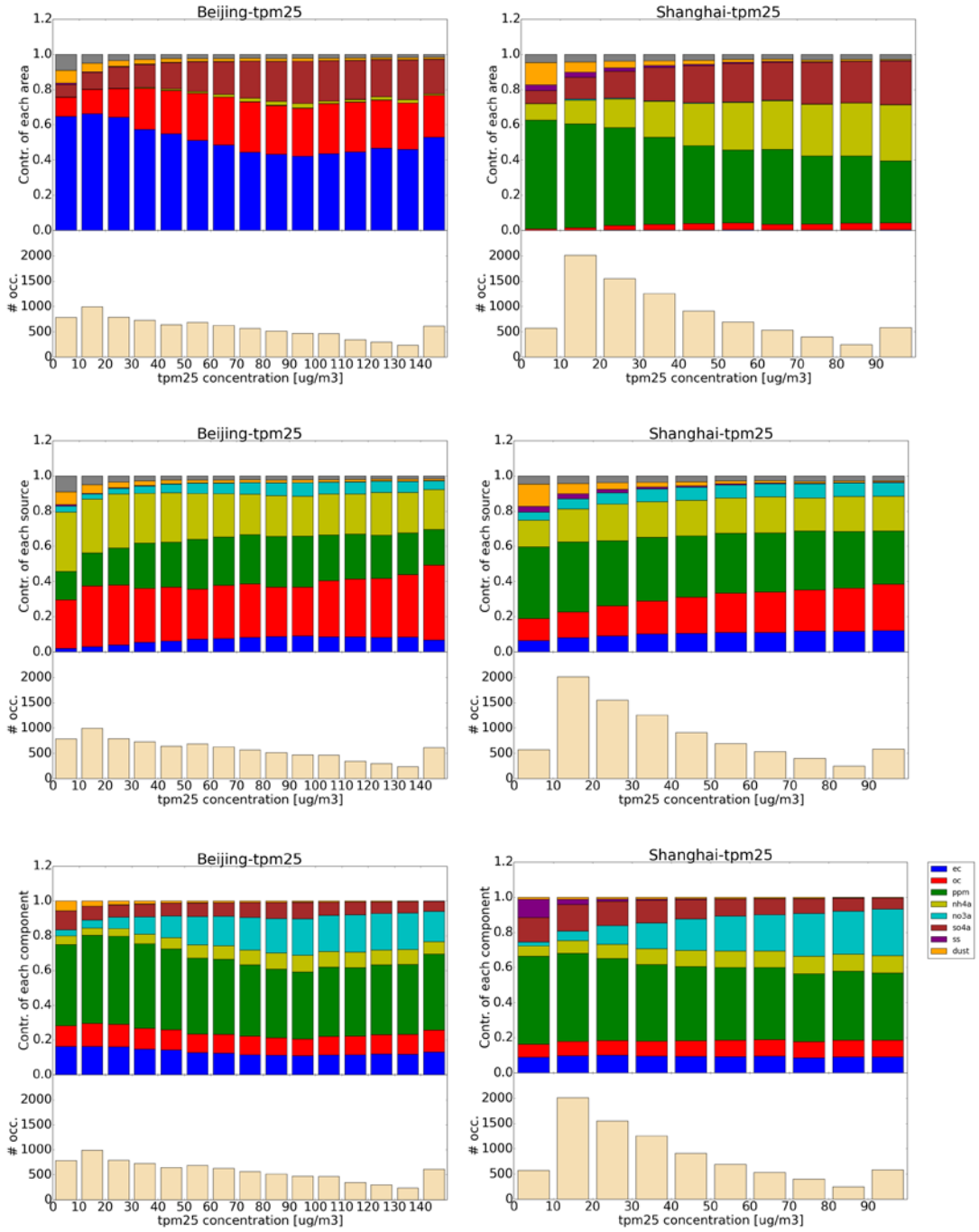

Figure 24 Dominant source areas, source categories and aerosol components as function of PM2.5 concentration for Beijing (left column) and Shanghai (right column)

The results are comparable to experimental source apportionment studies (Wei et al., 2015; Yu, 2013; Zhou et al., 2016; Zíková et al., 2016).
Note that road dust resuspension (Bi et al., 2007; Yu, 2013) and other local sources such as construction and demolition works (Chen et al., 2007) are not incorporated into the LOTOS-EUROS modelling framework for China yet but may also be important. These contributions would lower the bias between model and observations and enhance the urban contribution. Another process unaccounted for in the present model version is secondary organic aerosol formation. Secondary organic aerosol, with major contributions from anthropogenic fossil fuel combustion, may largely contribute to urban organic matter levels (Cao et al., 2013). It is to be expected that the secondary nature of SOA may favour transport and relatively low urban contributions.

In addition to annual analyses of the source contributions, the source apportionment system can also be applied to evaluate the dominant sources for specific events. Figure 26 shows the sectoral and regional contributions for a time period in January and one in August 2013 in Beijing. The first winter period is dominated by local residential combustion emissions, while for the second period, there is a mix of contributing sectors: industry, transport, power sector and even agricultural and natural sources have considerable contributions for some of the peaks. The local contribution for this period is also much smaller and pollution transported from surrounding provinces or even further away have become more important.

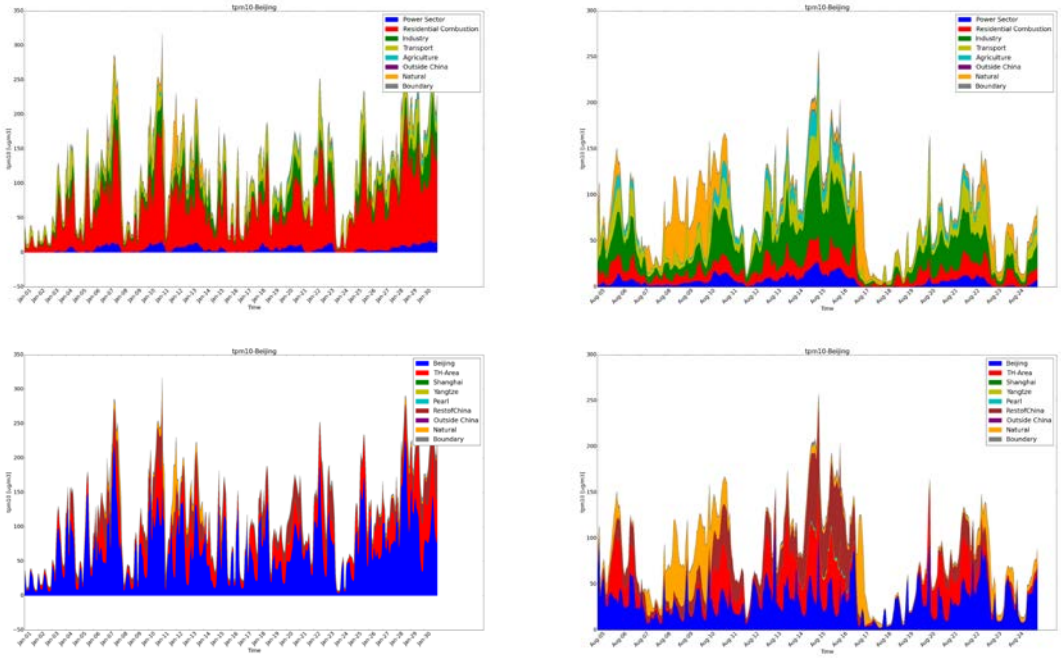

Figure 25 Contribution per source category (upper plots) and region (lower plots) for PM10 for an episode in January 2013 (left) and August 2013 in Beijing.

II.4 Conclusion source apportionment

The source attribution shows that on average about half of the PM2.5 pollution in both cities originates from the municipality itself. About a quarter of the PM2.5 comes from the neighbouring provinces whereas the remaining quarter is attributed to long range transport from anthropogenic and natural components. Residential combustion, transport, and industry are identified as the main sources with comparable contributions allocated to these sectors. The importance of the sectors varies throughout the year and differs slightly between the cities. During winter urban contributions from residential combustion are dominant, whereas industrial and traffic contributions with a larger share of regional transport dominate the source apportionment during summer. These results are in agreement with previous source apportionment studies and show that for mitigation strategies to be effective they should focus on several sectors and combine both local and regional scale measures.

The LOTOS-EUROS system proves to be a powerful tool for policy support applications outside Europe as the intermediate complexity of the model allows the assessment of the area and sector of origin over long time periods.

References

Banzhaf, S., Schaap, M., Kranenburg, R., Manders, A.M.M., Segers, A.J., Visschedijk, A.J.H., Van Der Gon, H.A.C.D., Kuenen, J.J.P., Van Meijgaard, E., Van Ulft, L.H., Cofala, J., Builtjes, P.J.H., 2015. Dynamic model evaluation for secondary inorganic aerosol and its precursors over Europe between 1990 and 2009. Geosci. Model Dev. 8, 1047–1070. doi:10.5194/gmd-8-1047-2015

Batterman, S., Xu, L., Chen, F., Chen, F., Zhong, X., 2016. Characteristics of PM2.5 concentrations across Beijing during 2013–2015. Atmos. Environ. 145, 104–114. doi:10.1016/j.atmosenv.2016.08.060

Bi, X., Feng, Y., Wu, J., Wang, Y., Zhu, T., 2007. Source apportionment of PM10 in six cities of northern China. Atmos. Environ. 41, 903–912. doi:10.1016/j.atmosenv.2006.09.033

Boersma, K.F., Eskes, H.J., Dirksen, R.J., van der A, R.J., Veefkind, J.P., Stammes, P., Huijnen, V., Kleipool, Q.L., Sneep, M., Claas, J., Leitão, J., Richter, A., Zhou, Y., Brunner, D., 2011. An improved tropospheric NO_2 column retrieval algorithm for the Ozone Monitoring Instrument. Atmos. Meas. Tech. 4, 1905–1928. doi:10.5194/amt-4-1905-2011

Builtjes, P.J.H., van Loon, M., Schaap, M., Teeuwisse, S., Visschedijk, A.J.H. and Bloos, J.P., 2003. Project on the modelling and verification of ozone reduction strategies: contribution of TNO-MEP, TNO report MEP-R2003/166. Apeldoorn, The Netherlands.

Cao, J.J., Zhu, C.S., Tie, X.X., Geng, F.H., Xu, H.M., Ho, S.S.H., Wang, G.H., Han, Y.M., Ho, K.F., 2013. Characteristics and sources of carbonaceous aerosols from Shanghai, China. Atmos. Chem. Phys. doi:10.5194/acp-13-803-2013

Chen, D.S., Cheng, S.Y., Liu, L., Chen, T., Guo, X.R., 2007. An integrated MM5-CMAQ modeling approach for assessing trans-boundary PM10 contribution to the host city of 2008 Olympic summer games-Beijing, China. Atmos. Environ. 41, 1237–1250. doi:10.1016/j.atmosenv.2006.09.045

Dammers, E., Palm, M., Van Damme, M., Vigouroux, C., Smale, D., Conway, S., Toon, G.C., Jones, N., Nussbaumer, E., Warneke, T., Petri, C., Clarisse, L., Clerbaux, C., Hermans, C., Lutsch, E., Strong, K., Hannigan, J.W., Nakajima, H., Morino, I., Herrera, B., Stremme, W., Grutter, M., Schaap, M., Wichink Kruit, R.J., Notholt, J., Coheur, P.-F., Erisman, J.W., 2016. An evaluation of IASI-NH3 with ground-based FTIR measurements. Atmos. Chem. Phys. Discuss. 2016, 1–30. doi:10.5194/acp-2016-141

European Commission, Joint Research Center (JRC), Netherlands Environmental Assessment Agency (PBL), 2011. Emission Database for Global Atmospheric Research (EDGAR) [WWW Document]. release version 4.2. URL http://edgar.jrc.ec.europa.eu

Flemming, J., Inness, a., Flentje, H., Huijnen, V., Moinat, P., Schultz, M.G., Stein, O., 2009. Coupling global chemistry transport models to ECMWF's integrated forecast system. Geosci. Model Dev. Discuss. 2, 763–795. doi:10.5194/gmd-2-253-2009

Guenther, A., Karl, T., Harley, P., Wiedinmyer, C., Palmer, P.I., Geron, C., 2006. Estimates of global terrestrial isoprene emissions using MEGAN (Model of Emissions of Gases and Aerosols from Nature). Atmos. Chem. Phys. 6, 3181–3210.

Hendriks, C., Kranenburg, R., Kuenen, J., van Gijlswijk, R., Wichink Kruit, R., Segers, A., Denier van der Gon, H., Schaap, M., 2013. The origin of ambient particulate matter concentrations in the Netherlands. Atmos. Environ. 69, 289–303. doi:10.1016/j.atmosenv.2012.12.017

Hendriks, C., Kranenburg, R., Kuenen, J.J.P., Van den Bril, B., Verguts, V., Schaap, M., 2016. Ammonia emission time profiles based on manure transport data improve ammonia modelling across north western Europe. Atmos. Environ. 131, 83–96. doi:10.1016/j.atmosenv.2016.01.043

Hu, J., Chen, J., Ying, Q., Zhang, H., 2016. One-year simulation of ozone and particulate matter in China using WRF/CMAQ modeling system. Atmos. Chem. Phys. 16, 10333–10350. doi:10.5194/acp-16-10333-2016

Huang, R.J., Zhang, Y., Bozzetti, C., Ho, K.F., Cao, J.J., Han, Y., Daellenbach, K.R., Slowik, J.G., Platt, S.M., Canonaco, F., Zotter, P., Wolf, R., Pieber, S.M., Bruns, E.A., Crippa, M., Ciarelli, G., Piazzalunga, A., Schwikowski, M., Abbaszade, G., Schnelle-Kreis, J., Zimmermann, R., An, Z., Szidat, S., Baltensperger, U., El Haddad, I., Prevot, A.S., 2014. High secondary aerosol contribution to particulate pollution during haze events in China. Nature 514, 218–222. doi:10.1038/nature13774

Kaiser, J.W., Heil, A., Andreae, M.O., Benedetti, A., Chubarova, N., Jones, L., Morcrette, J.-J., Razinger, M., Schultz, M.G., Suttie, M., van der Werf, G.R., 2012. Biomass burning emissions estimated with a global fire assimilation system based on observed fire radiative power. Biogeosciences 9, 527–554. doi:10.5194/bg-9-527-2012

Kranenburg, R., Segers, a. J., Hendriks, C., Schaap, M., 2013. Source apportionment using LOTOS-EUROS: module description and evaluation. Geosci. Model Dev. 6, 721–733. doi:10.5194/gmd-6-721-2013

Lang, J., Cheng, S., Li, J., Chen, D., Zhou, Y., Wei, X., Han, L., Wang, H., 2013. A monitoring and modeling study to investigate regional transport and characteristics of PM2.5 pollution. Aerosol Air Qual. Res. 13, 943–956. doi:10.4209/aaqr.2012.09.0242

Levy, R., Hsu, C., 2015. MODIS Atmosphere L2 Aerosol Product. NASA MODIS Adaptive Processing System [WWW Document]. URL http://dx.doi.org/10.5067/MODIS/MOD04_L2.006

Li, L., An, J.Y., Zhou, M., Yan, R.S., Huang, C., Lu, Q., Lin, L., Wang, Y.J., Tao, S.K., Qiao, L.P., Zhu, S.H., Chen, C.H., 2015. Source apportionment of fine particles and its chemical components over the Yangtze River Delta, China during a heavy haze pollution episode. Atmos. Environ. 123, 415–429. doi:10.1016/j.atmosenv.2015.06.051

Manders, A., Builtjes, P., Curier, L., Denier van der Gon, H., Hendriks, C., Jonkers, S., Kuenen, J., Timmermans, R., Wichink Kruit, R.A., van Pul, A., Sauter, F., van der Swaluw, E., Douros, J., Eskes, H., van Meijgaard, E., van Ulft, B., Mues, A., Banzhaf, S., Schaap, M., 2016. Curriculum Vitae of the LOTOS-EUROS chemistry transport model (v1.11). Geosci. Model Dev. submitted.

Manders, A.M.M., Schaap, M., Querol, X., Albert, M.F.M.A., Vercauteren, J., Kuhlbusch,

T.A.J., Hoogerbrugge, R., 2010. Sea salt concentrations across the European continent. Atmos. Environ. 44, 2434–2442. doi:10.1016/j.atmosenv.2010.03.028

Schaap, M., Kranenburg, R., Curier, L., Jozwicka, M., Dammers, E., Timmermans, R., 2013. Assessing the sensitivity of the OMI-NO2 product to emission changes across europe. Remote Sens. 5, 4187–4208.

Stern, R., Builtjes, P., Schaap, M., Timmermans, R., Vautard, R., Hodzic, A., Memmesheimer, M., Feldmann, H., Renner, E., Wolke, R., Kerschbaumer, A., 2008. A model inter-comparison study focussing on episodes with elevated PM10 concentrations. Atmos. Environ. 42, 4567–4588. doi:10.1016/j.atmosenv.2008.01.068

Timmermans, R. Kranenburg, R., Manders, A., Hendriks, C., Segers, A., Dammers, E., Zhang, Q., Wang, L., Liu, Z., Denier van der Gon, H., Schaap, M., 2016. Source apportionment of PM2.5 across China using LOTOS-EUROS. Atmos. Environ. submitted.

US EPA, 2004. Air Quality Criteria for Particulate Matter [WWW Document]. URL https://cfpub.epa.gov/ncea/risk/recordisplay.cfm?deid=87903

Van Damme, M., Clarisse, L., Heald, C.L., Hurtmans, D., Ngadi, Y., Clerbaux, C., Dolman, A.J., Erisman, J.W., Coheur, P.F., 2014a. Global distributions, time series and error characterization of atmospheric ammonia (NH3) from IASI satellite observations. Atmos. Chem. Phys. 14, 2905–2922. doi:10.5194/acp-14-2905-2014

Van Damme, M., Wichink Kruit, R.J., Schaap, M., Clarisse, L., Clerbaux, C., Coheur, P.F., Dammers, E., Dolman, A.J., Erisman, J.W., 2014b. Evaluating 4 years of atmospheric ammonia (NH3) over Europe using IASI satellite observations and LOTOS-EUROS model results. J. Geophys. Res. Atmos. 119, 9549–9566. doi:10.1002/2014JD021911

Wagstrom, K.M., Pandis, S.N., Yarwood, G., Wilson, G.M., Morris, R.E., 2008. Development and application of a computationally efficient particulate matter apportionment algorithm in a three-dimensional chemical transport model. Atmos. Environ. 42, 5650–5659. doi:10.1016/j.atmosenv.2008.03.012

Wei, Z., Wang, L., Ma, S., Zhang, F., Yang, J., 2015. Source Contributions of PM2.5 in the Severe Haze Episode in Hebei Cities. Sci. World J. 2015, 11. doi:10.1155/2015/480542

Yu, L., 2013. Characterization and Source Apportionment of PM2.5 in an Urban Environment in Beijing. Aerosol Air Qual. Res. 13, 574–583. doi:10.4209/aaqr.2012.07.0192

Zhang, L., Liu, L., Zhao, Y., Gong, S., Zhang, X., Henze, D.K., Capps, S.L., Fu, T.-M., Zhang, Q., Wang, Y., 2015. Source attribution of particulate matter pollution over North China with the adjoint method. Environ. Res. Lett. 10, 84011. doi:10.1088/1748-9326/10/8/084011

Zhou, J., Xing, Z., Deng, J., Du, K., 2016. Characterizing and sourcing ambient PM2.5 over key emission regions in China I: Water-soluble ions and carbonaceous fractions. Atmos. Environ. 135, 20–30. doi:10.1016/j.atmosenv.2016.03.054

Zíková, N., Wang, Y., Yang, F., Li, X., Tian, M., Hopke, P.K., 2016. On the source contribution to Beijing PM2.5 concentrations. Atmos. Environ. 134, 84–95. doi:10.1016/j.atmosenv.2016.03.047